PNAS RESEARCH ARTICLE | SYSTEMS BIOLOGY

The dynamic response of the bacterial flagellar motor to its direct intracellular input signal

Alina M. Vrabioiu[a], Basarab G. Hosu[a], and Aravinthan D. T. Samuel[a,1]

Edited by William Bialek, Princeton University, Princeton, NJ; received June 20, 2025; accepted January 16, 2026

The bacterial flagellar motor drives bacterial swimming and chemotaxis by rotating helical flagellar filaments. When *Escherichia coli* navigates chemical gradients, the motor switches from counterclockwise (CCW) during forward swimming to clockwise (CW) during direction-changing tumbles. The motor responds indirectly to extracellular chemosensory input to membrane-bound chemoreceptors using an intervening intracellular signaling pathway. How the motor responds to its direct input signal—the diffusible messenger phosphorylated CheY (CheY-P)—remains poorly understood. Steady-state motor measurements have been modeled as an allosteric switch between CCW/CW states that depends on mean CheY-P levels. Allosteric models have suggested that as many as 20 CheY-P molecules can be bound to the motor when it switches rotational direction. But steady-state models cannot predict the sensitivity of the motor to dynamic changes in CheY-P that essentially modulate chemotactic behavior. We present an optogenetic reagent that precisely controls the direct dynamical input signal to the motor. We designed a "caged" molecule, Opto-CheY, that is transiently activated by photon absorption. We find that activation and binding of one to three additional CheY-P molecules is sufficient to switch the motor from the CCW to CW state. The sensitivity of the motor to small changes in CheY-P occupancy helps resolve a long-standing paradox about the high sensitivity of the chemotactic response to external sensory input. Optogenetic biochemistry by light-activated uncaging of signal molecules is a new strategy to dissect information-processing in the living cell.

optogenetics | rate-limiting steps | CheY-P | Aslov2 | flagellar motor

Significance

Motile bacteria swim to better environments by modulating the rotation of the bacterial flagellar motor. How this motor responds to intracellular signaling activity is poorly understood. The physiologically relevant response of the motor is to transient activation of intracellular signaling molecules on the subsecond time scale of bacterial decision-making. Here, we report an optogenetic probe that targets in vivo the output module of the chemotactic network. We demonstrate that the motor has high dynamical sensitivity to the binding of single intracellular signaling molecules. This solves a long-standing problem of high sensitivity and signal amplification in the bacterial chemotactic response.

Chemotactic behavior in *Escherichia coli* is exquisitely sensitive. The binding of single chemoattractant molecules to membrane-bound chemoreceptors will modulate bacterial flagellar motor (BFM) rotation and swimming behavior (1–4). The complete transformation from sensory input to motor response is a convolution of multiple biochemical steps from chemoreceptor activation to motor switching between counterclockwise (CCW) and clockwise (CW) rotation. The physics of chemoreception allows membrane-bound receptors to reliably count single ambient chemoattractant molecules (1–3). However, it has been challenging to isolate and study specific information-processing steps and molecular interactions inside the cell. The last step—how the motor responds to its direct input signal, phosphorylated CheY (CheY-P)—remains poorly understood.

CheY-P is produced by CheA (kinase associated with chemoreceptors, Fig. 1*A*). CheY-P diffuses in the cytoplasm and binds to the C-ring, an intracellular component of the motor (5, 6). The C-ring is an oligomer made of $M = 34$ to 44 identical subunits, each a heteromer assembled from FliM, FliN, and FliG proteins (7–10). Thus, each CheY-P molecule diffuses and binds to one of M binding sites provided by FliM/FliN (8, 11). The chemotactic response depends on a large conformational change by the C-ring when enough binding sites are occupied by CheY-P (12, 13). The C-ring has different conformational states for CCW and CW motor rotation (14, 15).

Cluzel et al. (16) measured the steady-state CW bias (fraction of the total time the motor spends in the CW state) for cells with different steady-state [CheY-P]. Higher CheY-P levels correlated with higher CW bias, following a steep concentration dependence (Hill coefficient ~10 to 20) (16, 17). The steep Hill curve is often interpreted as a mechanism for signal amplification. Near inflection, a small difference in steady-state CheY-P levels corresponds to a large difference in steady-state CW bias.

However, steady-state measurements inform the thermodynamics of motor switching at equilibrium, not how the system responds to the transient perturbations of sensory transduction that are essential for chemotaxis up chemical gradients. To probe the kineticstructure of chemotactic signal processing, one needs to probe the motor response to defined perturbations of sensory input or intracellular signaling.

Author affiliations: [a]Department of Physics, Harvard University, Cambridge, MA 02138

Author contributions: A.M.V. and A.D.T.S. designed research; A.M.V. performed research; A.M.V. and B.G.H. contributed new reagents/analytic tools; A.M.V. analyzed data; and A.M.V. and A.D.T.S. wrote the paper.

The authors declare no competing interest.

This article is a PNAS Direct Submission.

[1]To whom correspondence may be addressed. Email: samuel@physics.harvard.edu.

This article contains supporting information online at https://www.pnas.org/lookup/suppl/doi:10.1073/pnas.2516278123/-/DCSupplemental.

Published March 3, 2026.

How sensitive is the motor to its direct input signal? How many additional CheY-P molecules bind to the motor when it switches from CCW to CW? The smallest input signal that evokes a CCW → CW switch should occur in a motor that is "dark-adapted" to low CheY-P levels. Analogous questions about the smallest quantal stimulus that triggers a behavioral response have been asked in visual neuroscience (18). How many photons are absorbed by the dark-adapted retina to see the dimmest flash? (19–21) How many photons are absorbed by the dark-adapted rod cell to evoke an electrical response? (22) Visual neuroscientists decisively answered these questions to establish single-photon sensitivity in vertebrate vision.

To date, it has only been possible to indirectly change CheY-P levels using external chemosensory input. But any effect of external input on internal CheY-P is confounded by the intracellular signaling network. Cell-to-cell variability and stochasticity throughout this network adds further uncertainty when interpreting the motor response to external input (23, 24). Here, we present an optogenetic approach to directly probe the sensitivity limits of the bacterial flagellar motor to its input signal.

Results

Optogenetic tools allow light-activated perturbations of cellular signals (25). We sought an optogenetic approach to directly manipulate CheY-P in the living cell. We wanted to decouple CheY-P activity from the endogenous signaling network, activate CheY-P with controlled light pulses, and monitor the bacterial flagellar motor (BFM) response in real-time.

Designing Opto-CheY. Chemotactic signaling processing in *E. coli* works on the ~1 to 3 s time-scale, the range of run lengths in free-swimming cells (26–28). For bacterial chemotaxis, a suitable optogenetic probe must exhibit a light-activated conformational change that recovers its dark-state within this time-scale (29, 30). We selected the LOV2 domain from *Avena sativa* (AsLOV2). The AsLOV2 domain contains an α-helix (Jα) that unfolds upon absorbing a blue photon (~450 nm) (31). Wild-type AsLOV2 recovers its dark state with ~50 s half-life (31). Rapidly refolding variants have been identified, including $AsLOV2_{N449S}$ [<1 s recovery (32)] and $AsLOV2_{V416T}$ [~2 s recovery (33, 34)].

Our goal was to design "caged" CheY by chimeric fusion with AsLOV2 (Fig. 1*B*). We wanted a molecule that would uncage when the Jα helix unfolds upon photon absorption. To build a stable chimeric structure, protein orientation can be constrained by fusing adjacent domains at junctures within the same α-helix (35). By adjusting the length of the α-helical juncture, the relative position and orientation of adjacent domains can also be fine-tuned. Here, we fused the Jα helix of circularly permuted AsLOV2 (cpAsLOV2) (36, 37) to the C-terminal α-helix of CheY.

We sought a dark-state structure where a low-affinity inhibitory peptide would effectively cage CheY by plugging its motor binding site. For the inhibitory peptide, we chose 16 amino-acids from FliM, the endogenous binding partner of CheY, which we fused to the C-terminus of cpAsLOV2 (11). We hypothesized that photon-triggered unfolding of the Jα helix would release the constraint on CheY and AsLOV2 orientation—this would remove the inhibitory peptide and expose the CheY active site. We used AlphaFold (38) to test the length of the α-helical juncture until we found a prediction where the CheY active site is plugged in the dark-state and unplugged in the lit-state. We call this molecule Opto-CheY (Fig. 1*B*).

Testing Opto-CheY in an Optimal Bacterial Strain. CheY does not bind the C-ring to promote CW rotation unless it is activated by phosphorylation to CheY-P. CheA is the kinase that acts on CheY. CheB is the demethylase that reduces CheA activity. CheZ is the phosphatase that dephosphorylates CheY-P (Fig. 1*A*) (39, 40). In cells lacking CheZ and CheB, intracellular CheY is completely phosphorylated (41). Thus, to maximize motor sensitivity to optogenetic activation, we expressed Opto-CheY in a Δ*cheB*Δ*cheZ*Δ*cheY* strain background.

Previous steady-state measurements found that the motor is most sensitive to CheY-P in its normal endogenous range, 2 to 4 μM (16). We titrated Opto-CheY levels using insulated, variable-strength bacterial promoters (42) and used fluorescence correlation spectroscopy (FCS) to verify that CheY expression is within endogenous range (*SI Appendix*, Fig. S1).

Using targeted mutations of promoter and/or ribosome binding sites, we fine-tuned Opto-CheY expression to an optimal level where optogenetic stimulation spans the full dynamic range of motor response, from nearly fully CCW rotation to fully CW rotation (*SI Appendix*, Tables S1 and S2).

To determine the rotational direction of single motors we used the tethered cell approach (43). To tether cells directly by hooks (Fig. 1*A*) we developed a "sticky" hook approach. Specifically, we increased the number of positive charges in a surface exposed loop of the flagellar hook protein FlgE. This promotes the hook's electrostatic interaction with the negatively charged glass surface (*Materials and Methods*) (44, 45). We tethered cells that express $Opto\text{-}CheY_{N449S}$ (strain number 638, *SI Appendix*, Table S1) onto microscope coverslips. Pulses of blue light (~100 μ J/cm^2) trigger single CCW → CW switching events in motors that rotate exclusively or almost exclusively in the CCW direction (Fig. 1*C* and *SI Appendix*, Fig. S2). In contrast, cells that do not express Opto-CheY (strain number 657, *SI Appendix*, Table S1) never respond with CW rotation (*SI Appendix*, Fig. S2 and Movies S1–S6). These observations establish that blue light activates Opto-CheY to bind to the motor and promote CW rotation.

Tethered cells that express $Opto\text{-}CheY_{N449S}$ have motors that are nearly exclusively CCW in dark-state (average CW bias 0.011 ± 0.0032 for strain number 638, *SI Appendix*, Table S1). We attribute low but nonzero CW bias in dark-state to dark-state equilibrium between folded and unfolded AsLOV2 (46, 47). This results in a population of Opto-CheY molecules that are active and can bind to the motor in the absence of optogenetic stimulation. If the motor reversals were indeed due to dark-state equilibrium, decreasing Opto-CheY expression should decrease the absolute amount of Opto-CheY molecules active in the dark and decrease the initial CW bias. When Opto-CheY expression level is decreased by ~ 20% via a base pair change in the ribosome binding site (48) dark-state CW bias decreased to 0.00185 ± 0.00064 (strain number 630, *SI Appendix*, Fig. S3). Conversely, when Opto-CheY expression is increased by ~33% with changes in both the ribosome binding and promoter sites dark-state CW bias increased to 0.085 ± 0.022 (strain number 670, *SI Appendix*, Fig. S3).

The CW bias of cells that express CheY and cpAsLOV2 without the inhibitory peptide (strain number 658, *SI Appendix*, Table S1) is 0.982 ± 0.0035 (Fig. 1*B* and *SI Appendix*, Fig. S3). We conclude that the entire range of the motor's response—from fully CCW in cells with caged Opto-CheY in the dark-state to fully CW in cells with constitutively active CheY-cpAsLOV2—can be spanned by optogenetic control.

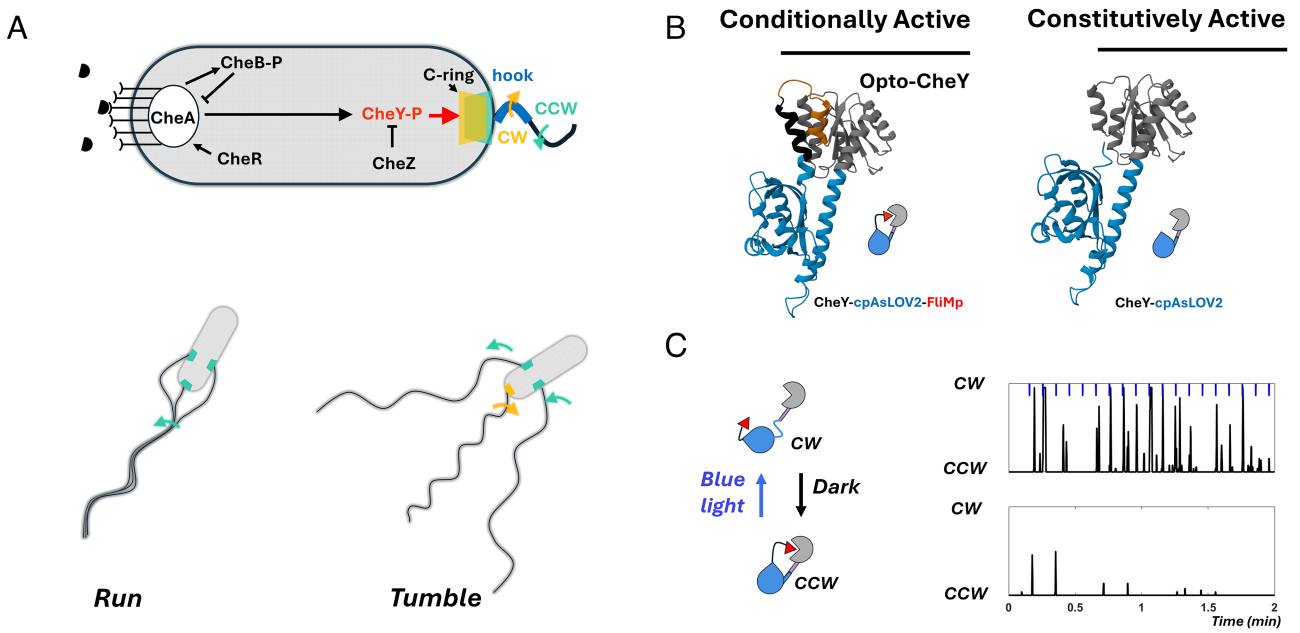

Fig. 1. Opto-CheY, a "caged," light-activated CheY. (*A*) Diagram of key molecules in the chemotaxis network. Extracellular ligands (black semicircles) bind to receptors and modulate the activity of CheA, the kinase that phosphorylates the diffusible messenger CheY. CheA activity adaptation is mediated by the methylase CheR and demethylase CheB. CheY-P binds to the C-ring and triggers a conformational change that results in BFM changing direction (CCW → CW). The swimming bacterium switches from a smooth run to a tumble. (*B*) AlphaFold structure predictions of chimeric molecules. Gray is *E. coli* CheY, blue is cpAsLOV2, black is a short linker, and orange is the FliM peptide. Cartoons depicting the "caged" dark-state of Opto-CheY and the constitutively active control are shown with the same color code. (*C*) Blue-light absorption triggers unfolding of the Jα helix, and CheY activation by removal of the FliM plug from the CheY active site. Active CheY binds to the C-ring and promotes the rotational switch of the BFM from CCW → CW. Light pulses (blue dots, ~100 μ J/cm^2) are applied every 6 s while monitoring BFM rotational state. Each response is a CW rotation (vertical black line) following a blue light pulse (blue dot) in an otherwise mostly CCW motor (bottom trace).

Quantal Stimulus at Response Threshold. The motor switches to CW rotation when enough CheY-P are added to the C-ring (49). Opto-CheY is transiently activated when it absorbs a single blue photon. By measuring when the motor "sees" an optogenetic pulse by switching from CCW → CW, we can estimate the minimum number of activated Opto-CheY that are added to the motor to trigger a switch.

In visual neuroscience, Hecht, Shlaer, and Pirenne (19) measured the minimum quantal stimulus at the retina—the number of rhodopsin molecules that must be activated by photons—for a dark-adapted human to see a dim flash of light. To do this, they made ingenious use of Poisson statistics. When the dark-adapted eye is exposed to dim flashes of light, each rhodopsin within the field of illumination has a small probability ($P \ll 1$) of absorbing a photon and contributing to "seeing." Because there are many rhodopsins ($N \gg 1$) that can potentially be activated, the probability that a specific number of rhodopsins are activated must follow Poisson statistics. A given light flash delivers a total number of photons per unit area (F, photons/cm^2) and activates on average a certain number of rhodopsins ($a = p \cdot N = (const \cdot F \cdot \sigma \cdot \Theta) \cdot N$), σ and Θ are the absorption cross-section and quantum yield of rhodopsin, *const* accounts for both efficiency in signal transductions and photon dissipation. From this, Poisson statistics defines the probability that any specific number of rhodopsins (k) are activated:

$$P_k = \frac{a^k e^{-a}}{k!} \qquad [1]$$

The probability that a flash evokes a behavioral response is the cumulative probability that the flash activates any number of rhodopsins above a threshold, θ:

$$P_{see} = \sum_{k=\theta}^{\infty} P_k = 1 - \sum_{k=0}^{\theta-1} P_k \qquad [2]$$

The average number of activated rhodopsins is proportional to flash intensity ($I = F/\tau$, where τ is the duration of the light pulse). Rearranging, $a = (const \cdot N \cdot \tau \cdot \sigma \cdot \Theta) \cdot I = \alpha \cdot I$, where α is constant for a given experimental system and

$$P_{see} = \sum_{k=\theta}^{\infty} \frac{(\alpha I)^k e^{-\alpha I}}{k!} = 1 - \sum_{k=0}^{\theta-1} \frac{(\alpha I)^k e^{-\alpha I}}{k!} \qquad [3]$$

When the probability of seeing is plotted against the natural logarithm of flash intensity ($\ln I$) a sigmoidal response curve will result. The slope of this curve at inflection depends strictly on θ (50). The steeper the curve, the higher the quantal threshold needed to "see" the flash.

Our experimental setup allows a similar approach (19–21, 51). Because the motor is nearly always in the CCW state in the dark, it tells us when it "sees" a pulse with a CCW → CW switch. Each cell has ~1,000 to 2,000 Opto-CheY (*SI Appendix*, Fig. S1) that are potentially activated by an optogenetic pulse ($N \gg 1$). Each Opto-CheY has a small probability of being activated and diffusing and binding to the motor ($P \simeq 0.005 \ll 1$, *SI Appendix*, Text). When a threshold number of additional Opto-CheY bind to the motor, they trigger a CCW → CW switch. By measuring motor response probability as a function of pulse intensity, we can leverage Poisson statistics to use Eq. **3** and estimate θ—the threshold, in our case, the minimum number of additional Opto-CheY molecules that must bind to the motor to trigger a response.

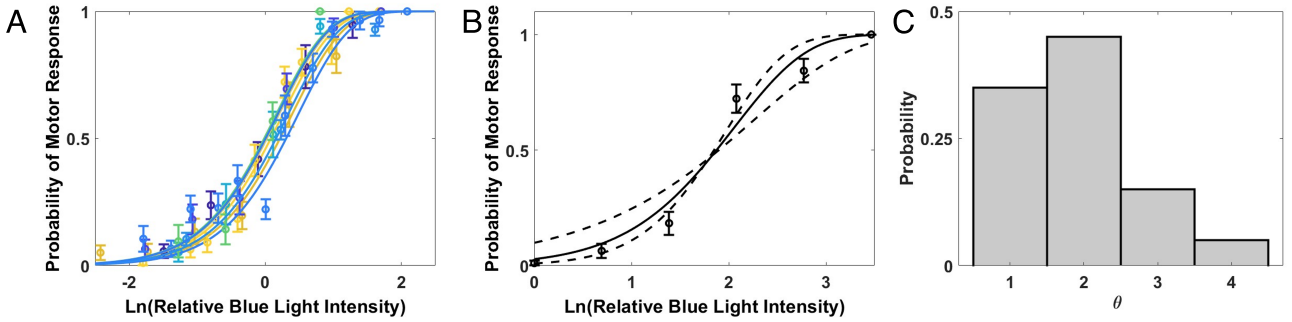

Fig. 2. Probability of motor response. (*A*) Opto-CheY$_{V416T}$-driven motor responses. Each motor is flashed with a series of pulses of increasing relative intensity ($I = I_{min} \cdot x$, $x = \{1, 2, 4, 8, 16, 32\}$, I_{min} delivers $\sim 7 \cdot 10^{12}$ blue photons/cm^2). Response probability for each BFM at a given intensity is calculated as the number of responses divided by the number of flashes. P_{see} with $\theta = 2$ is used to fit each dose–response curve (Eq. **3**). Ten individual BFM response curves and fits are shown translated horizontally relative to half-maximum response intensity. (*B*) The dose–response of one Opto-CheY$_{V416T}$ motor is shown along with best fit curves for fixed values of θ: $\theta = 2$ (black line), $\theta = 1$ (shallower dashed black line), $\theta = 3$ (steeper dashed black line). (*C*) A histogram of most probable θ for 20 individual BFM response curves, corresponding to the fit with highest R^2.

We tethered cells expressing Opto-CheY$_{V416T}$ in the Δ*cheB*Δ*cheZ*Δ*cheY* background (strain number 636, *SI Appendix*, Table S1). Here, we used the Opto-CheY variant with "lit" state half-life ~2 s to lengthen the time Opto-CheY is in the active, signaling state. This strain has the lowest expression level that evokes motor responses (average initial CW bias is 0.0012 ± 0.0004). We selected motors with initial dark-state CW bias close to 0.001 (2 to 5 reversals per minute). Thus, the dark-state level of switching behavior in these motors, attributed to dark-state equilibrium between folded and unfolded Opto-CheY, is situated near the base of the response curve of previous steady-state experiments (16).

We applied blue-light flashes (2 ms) with geometrically increasing intensity ($I = I_{min} \cdot x$, $x = \{1, 2, 4, 8, 16, 32\}$, I_{min} flash delivers $\sim 7 \cdot 10^{12}$ blue photons/cm^2, *SI Appendix*, Fig. S4 and Movies S7 and S8). The frequency of the flashes is constant for a given intensity (0.25 Hz, every 4 s, for I_{min}). The interval between flashes was chosen such that each motor response is independent of the previous response (according to criteria outlined in *SI Appendix*, Text and Figs. S5 and S6). The minimum interval that satisfies the criteria is a function of flash intensity; the stronger flash requires a longer time interval to recover the baseline (0.0667 Hz, every 15 s for the maximum flash intensity, *SI Appendix*, Fig. S4). At each intensity, we estimate response probability (P = # of flashes that trigger a CCW → CW switch divided by # total flashes). We plotted response probability versus the logarithm of relative flash intensity (Fig. 2).

We fitted the data for each motor to Eq. **3** (*SI Appendix*, Text). Best fits are in the range $\theta = 1$ to 3 for all but one motor (Fig. 2*C*). Fig. 2*A* shows 10 individual motor responses (motors 1 to 10 in *SI Appendix*, Table S5) along with corresponding $\theta = 2$ fits. Individual responses/fits are translated horizontally so they align to the half maximal response and highlight the steepness of the curves (raw responses are shown in *SI Appendix*, Fig. S8).

For single motors, the cumulative Poisson function is often fit to slightly different values of θ with similar R^2 values (*SI Appendix*, Table S5). For example, $\theta = 2$ is the best fit for the motor response shown in Fig. 2*B*, but $\theta = 3$ fit is a close second, suggesting measurement uncertainty of $\theta \pm 1$. In our model, θ is an estimate of the number of Opto-CheY that must be activated and added to the motor to reach the threshold of CCW → CW switching. Differences in θ can also be attributed to differences in dark-state Opto-CheY occupancy. Indeed, we found that motors that start at higher initial biases (motors 11 to 20 in *SI Appendix*, Table S5) have higher response probability at the lowest blue light intensity (y-axis intercepts above 0.1 in *SI Appendix*, Fig. S8, V416T panel) as well as flatter overall responses that are best fit with a $\theta = 1$ (*SI Appendix*, Table S5). Other Opto-CheY strains with higher dark-state CW bias were also best fit by shallowed cumulative Poisson functions with low θ values (strain number 638, *SI Appendix*, Fig. S9*C* and its caption).

Opto-CheY$_{V416T}$ recovers its dark-state in ~2 s after activation (33). Opto-CheY$_{N449S}$ recovers faster, in <1 s (32). We measured similar dose–response curves using Opto-CheY$_{N449S}$ (strain numbers 630 and 638, *SI Appendix*, Table S1). Increasing light intensity led to increasing response probability with similar steepness (θ~2) (*SI Appendix*, Figs. S8 and S9). However, response probability with the shorter-lived probe did not always saturate close to 1 even with the strongest light pulses (*SI Appendix*, Fig. S7). Rapid inactivation puts an upper bound on response probabilities. If Opto-CheY molecules refold before enough have time to bind the C-ring, no response can be evoked. Consistent with this idea, the motor can respond to every stimulation of Opto-CheY$_{N449S}$ when longer light pulses of lower intensity are used, which effectively increases the lifetime of the probe (*SI Appendix*, Fig. S10).

The Impulse Response of the Motor. In classic impulse response measurements, tethered cells were exposed to short pulses of chemoattractant from an iontophoretic pipette (26, 27). These cells expressed wild-type CheY at endogenous levels and had higher initial CW bias. Following each iontophoretic pulse, CCW likelihood rises for ~1 s, returns to baseline, falls below baseline, and finally returns to baseline after ~3 s. This biphasic response reveals the time-scale of chemotactic signal processing. This response time-course is a mathematical convolution of all signaling events from chemoreceptor activation to motor switching.

Optogenetic activation of Opto-CheY allows us to measure the kinetics of the last event in the signaling pathway, the interaction of CheY-P with the C-ring. Because nearly every CCW → CW switch is light-evoked, each response is characterized by two time intervals. Latency is the interval between the optogenetic pulse and the CCW → CW switch (the time it takes for the flash to evoke a response). Duration is the interval between the first CCW → CW switch and the return to the CCW state (more precisely, the duration of the first CW interval following the flash, Fig. 3*A*). As in the classic impulse response experiments (26, 27), the average of single motor binary traces following blue light stimulation generates the probability of being in the CW state at a given time after the light pulse (Fig. 3*A*).

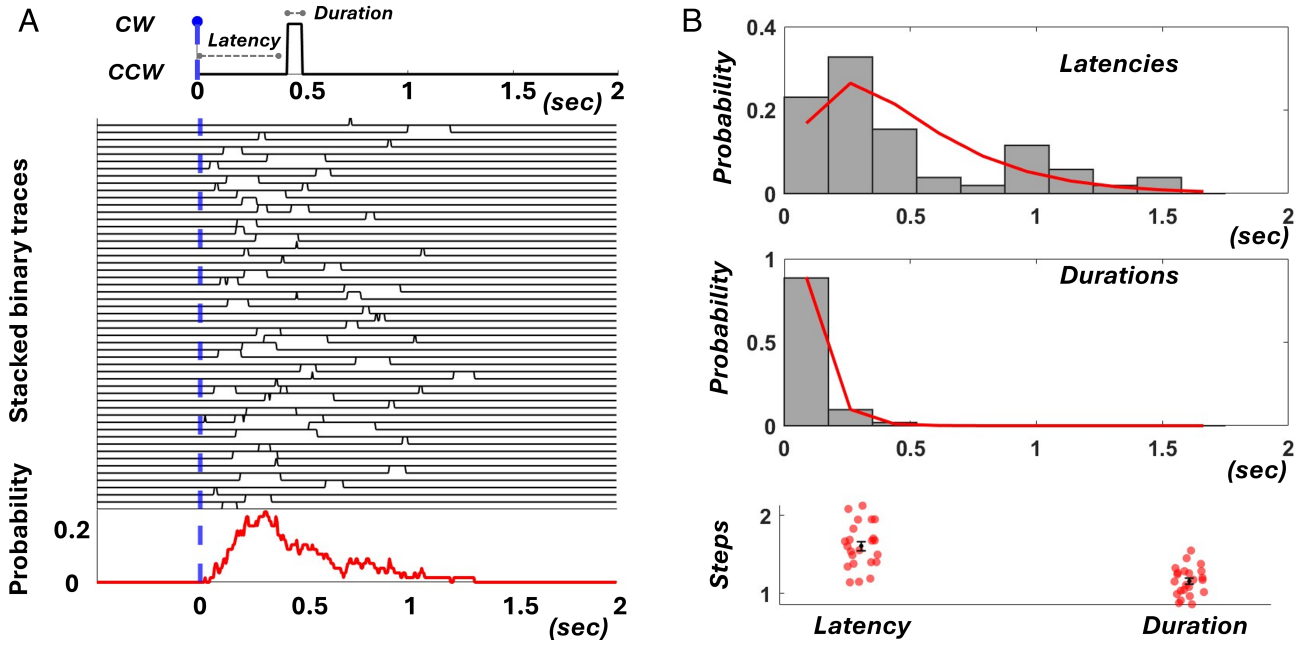

Fig. 3. Impulse response of the motor. (*A*) Each response is decomposed into the time it takes to respond (Latency), and the duration of the first CW interval (Duration). Opto-CheY$_{N449S_{higher}}$ motor is subjected to 400 ~blue light pulses ($I = I_{min} \cdot x$, $x = 4$) and responded 54 times (response probability=0.135). The 54 positive trials are aligned relative to the blue-light pulse and averaged to generate the likelihood of being in the CW state at a given time after the pulse (*Bottom*, red). (*B*) Histograms of the 54 latencies and durations are shown (normalized to represent probabilities). Latencies are fit with a gamma function (shape parameter 2, $n = 2$). Durations are fit with an exponential function (shape parameter 1, $n = 1$). Different BFM responses are each fitted to estimate the number of rate limiting steps for latency and duration. Individual points, means, and SEs are shown.

The statistics of the optogenetically induced switching response reflect the stochastic nature of CheY-binding kinetics. Fluctuations in response latency (e.g., the time it takes to reach the CW state, latency in Fig. 3*A*) can be informative about elementary steps in the overall biochemical reaction (52–54). An elementary, single-step reaction is a Poisson process with exponentially distributed completion times. For a multistep reaction mechanism (multiple, sequential elementary steps) the distribution of overall reaction times is given by the convolution of its elementary steps duration distributions, dominated by the slowest steps (54). For n comparable, rate-limiting steps, the probability distributions of total reaction times are best fit by gamma functions with shape parameter equal to n.

We collected statistics for latency and duration using cells that express Opto-CheY$_{N449S_{higher}}$ (half-life <1 s, strain number 638, *SI Appendix*, Table S1) at different flash intensities. For the cell shown in Fig. 3*A*, 400 blue light pulses were applied ($I = I_{min} \cdot x$, $x = 4$), and the motor responded 54 times (response probability = 0.135). Histograms of 54 response latencies and durations are shown in Fig. 3*B*. For a weak stimulus with low response probability (13.5% of flashes evoke a reversal), response latency is a significant proportion of the overall signal processing time (Fig. 3*B*).

Probability distributions for latency are poorly fit by single-exponential curves. Response latency is better fit by the gamma distribution. Assuming that n rate-limiting steps with similar kinetics occur in series, n can be estimated from the best-fit gamma distribution.

When gamma distributions are fit to response latency histograms, we estimate n~2 for most cells (Fig. 3 *B*, *Bottom*). One possibility is that response latency is the result of two rate limiting steps—such as the activation and successive binding of two Opto-CheY molecules to reach the CW state of the motor. However, the probability distributions for the first CW interval duration at low flash intensity are well fit by single-exponential curves (Fig. 3*B*). Response duration might be the result of one rate-limiting step if only one Opto-CheY needs to unbind to return the motor to the CCW state.

Higher intensity flashes evoke higher motor response probabilities (Fig. 2 and *SI Appendix*, Figs. S8 and S9) presumably because they activate a higher number of Opto-CheY molecules. Response latency and duration are also modulated by stimulus strength (Fig. 4*A*). Mean latency and duration for a stimulus with ~14% response probability ($x = 4$) are 0.5 ± 0.05 s and 0.11 ± 0.013 s, respectively. For a stimulus with ~68% response probability ($x = 16$), mean response latency drops to 0.18 ± 0.015 s and mean response duration rises to 0.16 ± 0.016 s (Fig. 4*A*). This trend is consistent across 24 motors that we studied with both weak and strong stimuli—the stronger the stimulus, the shorter the latency and the longer the duration of a response.

Fig. 4*B* shows single motor responses at a given stimulus strength as points in the latency-duration space. Arrows connect the response to the weaker stimulus and the response to the stronger stimulus for single motors. Differences in the slopes of the lines reflect differences in individual motor dynamic responses. Increases in stimulus strength are correlated with decreases in latencies and increases in response duration, with different contributions across different motors. The same trend is observed in Opto-CheY$_{V416T}$ motors (half-life ~2 s, *SI Appendix*, Fig. S11). However, the Opto-CheY$_{V416T}$ motors take longer to return to the prestimulus baseline due to a longer lived perturbation.

Discussion

The chemotactic signaling pathway in *E. coli* has long been noted for high gain and sensitivity—small changes in chemoreceptor occupancy cause large changes in bacterial flagellar motor (BFM)

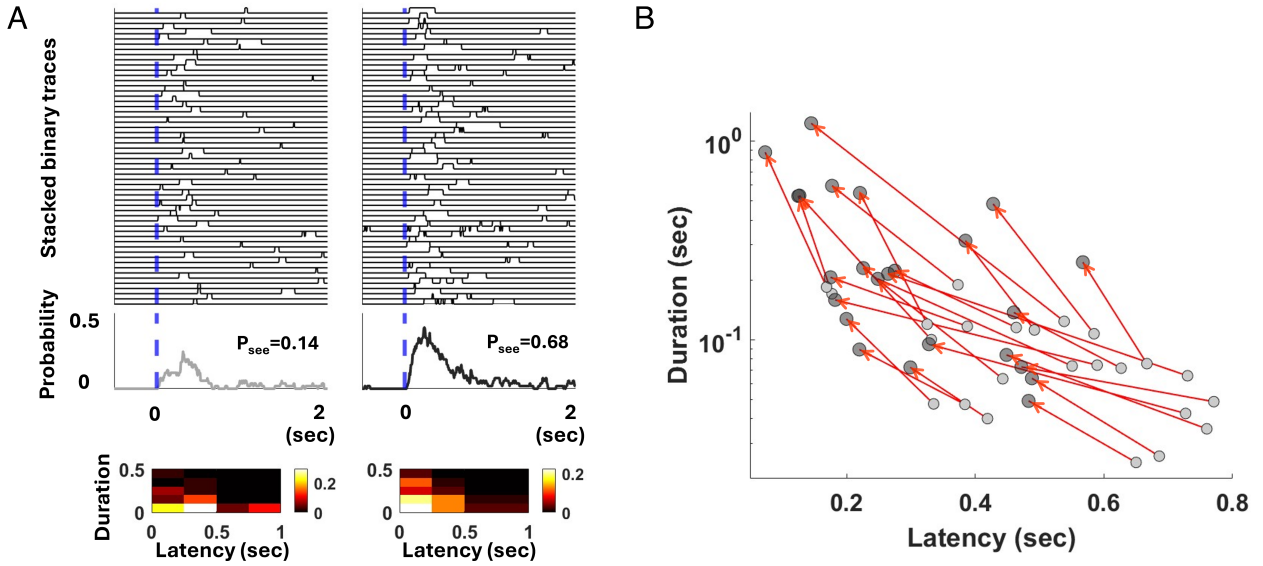

Fig. 4. Motor response to weak and strong stimuli. (*A*) Opto-CheY$_{N449S_{higher}}$ A single motor is subjected to 400 weak light pulses ($I = I_{min} \cdot x$, $x = 4$) and 120 strong pulses ($x = 16$). 57 responses for each stimulus are shown stacked and aligned relative to the light pulse (blue line). Average motor responses for each stimulus is shown (gray for weak; black for strong). Below, the 57 latencies and durations are used to generate a joint probability distribution shown as a 2D-histogram, and color coded for probability as shown in the color bar. (*B*) Average latencies and durations for the weak (gray) and strong (black) stimulus are shown for 24 motors. Red line interconnect responses of each motor, pointing toward the strong stimulus.

bias and swimming behavior. How the motor contributes to overall signal processing through its dynamical response has been poorly understood. Here, we studied the motor that is "dark"-adapted to low baseline CheY-P levels to probe the limit of molecular sensitivity. We report a dynamic sensitivity of the motor switching response to the binding of only 1 to 3 additional CheY-P molecules. In the regime of low baseline CheY-P levels, where motors rotate CCW, the high sensitivity of the motor to the binding of single signal molecules can contribute directly to signal amplification.

Previous theoretical and experimental work has suggested that the threshold of motor switching occurs near ∼50% occupancy of CheY-P binding sites (12, 13). However, the essential chemotactic response involves the adding and subtracting of small numbers of CheY-P molecules around the threshold of motor switching. Previous modeling has focused on the thermodynamics of conformational change and subunit coupling within the C-ring (12, 55). The dynamics of CheY-P occupancy near the switching threshold is not well-understood. Diffusion-limited binding at endogenous [CheY-P] is fast (∼10/s). CheY-P also unbinds at a rate of ∼10/s (12, 56, 57). A C-ring with M independent CheY-P binding sites can be modeled with $M + 1$ binding states (state i given by the number of occupied CheY-P binding sites). As the C-ring approaches the switching threshold from low occupancy, the kinetics will vary over time. As C-ring occupancy increases, the number of available binding sites decreases (site depletion), which should effectively decrease the "on" rate and increase the "off" rate of CheY-P binding to the motor. Thus, adding CheY-P molecules becomes rate-limiting as the motor advances from low occupancy to high occupancy states.

The motor was shown to adapt to changes in external load, as the mechanical load increases, more torque-generating stator units bind to the rotor (58), and CheY-P displays higher affinity for the C-ring (59). Changes in binding affinity can affect the dynamical response. Changes in binding affinity might not affect the binding occupancy near the switching threshold. The number of additional CheY-P molecules θ is likely to represent a diffusion-limited lower bound, reflecting the stochastic arrival of additional CheY-P molecules at the motor. This lower bound may be independent of upstream chemotactic signaling or downstream mechanical load. However, an increase in binding affinity might affect how fast the switching threshold is reached after stimulation, reflected in response latencies.

In our experiments, the motor initially has very low CW bias, low concentration of active CheY-P. The C-ring adaptively changes the number of binding sites in response to sustained changes in CheY-P levels (9). Therefore our motors are presumably adapted to low CheY-P levels. In addition, our tethered cells rotate slowly with motors adapted in the limit of high mechanical load. We conjecture that motors in our experiments are adapted both to high mechanical load and dark-state conditions. The adapted motor has to bind enough unfolded Opto-CheY in the dark-state to be near the switching threshold, and thereby maximally sensitive to optogenetically induced increase in Opto-CheY levels. Our estimates of θ in the cumulative Poisson functions (Fig. 2) and the nonexponential distribution of response latencies (Fig. 3) are both consistent with a small number of discrete rate-limiting steps to reach the switching threshold. The threshold number of CheY-P molecules that must be added to prior steady-state CheY-P occupancy corresponds to the number of rate-limiting binding events that trigger the switch.

In the regime of low baseline CheY-P levels, the high sensitivity of the motor to the binding of single signal molecules can contribute directly to signal amplification. Chemoreceptor-associated CheA molecules need only phosphorylate a small numbers of additional CheY molecules to trigger a tumbling response. The more CheY-P that is activated, the quicker the motor response. Two factors determine how many CheY-P must bind to the motor to evoke a CCW → CW switch: How many CheY-P are bound to the motor before the switch and how many more are needed to reach the threshold. Response latency is similarly dependent on these factors. The stronger the stimulus, the shorter the response latency.

Optogenetic activation of CheY-P allowed us to study the dynamics of the final reaction of the chemotaxis network for motors adapted to high load and low CheY-P concentrations. Our approach can be applied to other possible outputs in this system such as CheY-P fluorescence at the motor, which allows for linking CheY-P occupancy to switching probability. The approach can also be extended to motors at different loads and initial CW biases and eventually applied to the swimming cell under a variety of conditions that mimic physiologically relevant situations. This offers a way to test nonequilibrium theories of information-processing in bacterial chemotaxis (60–63). An advantage of our pipeline is that it offers a flexible and modular way to design optogenetic probes. We anticipate the extension of optogenetics to other proteins in the chemotactic signaling network (e.g., CheA, CheR, CheB). Our approach to inventing effective optogenetic probes is adaptable for in vivo dissection of intracellular signaling in diverse cell types.

Materials and Methods

***E. coli* Strains and Plasmid Construction.** Motile MG1655 strain is the parent strain in all experiments (64). Deletions of *cheB*, *cheZ*, *cheY*, *fliC*, *flgE*, and *fliK* were made sequentially, alone, and in combination (Δ*cheB*Δ*cheY*Δ*cheZ*) using the Datsenko and Wanner method with pKD3/pKD4 plasmids (65). An 85 bp scar remained after Flp/FRT recombination to eliminate the antibiotic resistance genes. Deletions were verified using PCR and Sanger sequencing of the PCR products. Bacterial strains are shown in *SI Appendix*, Table S1.

Opto-CheY Construction. *cheY* DNA coding sequence was amplified from *E. coli* genomic DNA; cpAsLOV2 synthesized as a G block by Invitrogen (*SI Appendix*, Table S4). Fragments with various linkers and truncations were assembled using the NEBuilder® HiFi assembly method (New England Biolabs) into the pEB2 plasmid backbone [Addgene #104007, kanamycin resistance and low-copy origin SC101 (66)] with a few modifications. Specifically, mutations were introduced to generate the series of pro1, pro3, proA, and pro5 promoters with increasing expression strength (42). The ribosome binding sites used were a T7 RBS variant (GAAGGAGgT) which reduces protein expression by ∼20% (48), and the wild type T7 RBS (*SI Appendix*, Table S2). Mutations (N449S,V416T) were introduced via PCR (numbering as in AsLOV2 sequence, consistent with previous publications). Plasmids are shown in *SI Appendix*, Table S2. Protein sequences are shown in *SI Appendix*, Table S3.

Sticky Hook Construction. We based the design of "sticky hooks" on a previous insertion of the AviTag protein sequence into the flagellar hook protein FlgE (*FlgE_C_Avi*) (44, 45). There are 3 surface-exposed, negatively charged AviTag amino-acids (GLN**D**IF**E**AQKI**E**WHE, *SI Appendix*, Fig. S12). We replaced these amino-acids with 3 positively charged ones (GLN**R**IF**R**AQKI**R**WHE) to promote interaction with the negatively charged glass surface (*SI Appendix*, Table S3). The modified sequence was introduced via PCR into *flgE* amplified from genomic DNA to generate $FlgE_{AviRRR}$ which was placed into the pTrc99A plasmid (67).

Cell Preparation and Attachment to Glass Slides. Cells for microscopy were inoculated in tryptone broth (TB) with necessary antibiotics at 1:1,000 dilution and grown at 27 °C till $OD_{600} = 0.55$ to 0.6. Leaky expression of $FlgE_{AviRRR}$ in the pTrc99A plasmid was sufficient for attachment in the MG1655 strains. Cells were spun down, washed, and resuspended in motility buffer with no salt (10 mM K_2HPO_4/KH_2PO_4, 100 μM EDTA, 10 mM lactate, pH = 7). Cells were then added to channel slides (made by combining a glass slide, 2 layers of sticky tape, and coverslip) and allowed to settle for 5 to 10 min on the coverslip. After thorough washing (∼0.5 to 1.0 mL of motility buffer), the tethered cells were used for experiments.

Microscope Setup and Imaging Assay. We used a Nikon Eclipse Ti-U microscope and an Apo 60X oil objective (NA 1.49). The epifluorescence port was used to attach the blue-light LED for optogenetic stimulation. Neutral density filters (NDx reduce light intensity by $1/x$, $x = 1, 2, 4, 8, 16, 32$) were used to modulate the intensity of the blue light pulse. Phase contrast images were acquired using a FLIR camera at 200 frames per second. A yellow filter was placed in front of the phase contrast lamp to filter out unwanted blue light during image acquisition. The LED-generated blue light pulse transiently increases the intensity of the frames it overlaps during phase contrast acquisition (1 to 2 frames, depending on pulse positioning and intensity). This pinpoints the localization of blue light pulses during image analysis. Trains of short pulses (2 to 5 ms) at each light intensity were applied every 2 to 15 s.

Image Processing and Data Fitting. Phase contrast movies were analyzed using ImageJ and Matlab with custom software. Each frame was assigned a rotational direction (CCW/CW), and CW bias was calculated as the number of CW frames divided by the total frames in a given time interval. Response probabilities were computed as P = # of flashes that trigger a CCW → CW switch divided by # total flashes of a given intensity.

Data, Materials, and Software Availability. All data and code supporting this study are available at Zenodo (DOI: 10.5281/zenodo.18635164) (68). The plasmids described here are available from Addgene (plasmid nos. 253255–253260 and 253285–253286) (69).

ACKNOWLEDGMENTS. This work was supported by NSF (award number 2146519) and Dean's Competitive Fund at Harvard University. We are grateful to Thierry Emonet, Phillipe Cluzel, and members of the Samuel lab for discussions and support.

1. H. C. Berg, E. M. Purcell, Physics of chemoreception. *Biophys. J.* **20**, 193–219 (1977).
2. U. Alon, M. G. Surette, N. Barkai, S. Leibler, Robustness in bacterial chemotaxis. *Nature* **397**, 168–171 (1999).
3. W. Bialek, S. Setayeshgar, Physical limits to biochemical signaling. *Proc. Natl. Acad. Sci. U.S.A.* **102**, 10040–10045 (2005).
4. H. C. Berg, *E. coli in Motion* (Springer, New York, 2004).
5. S. Ravid, P. Matsumura, M. Eisenbach, Restoration of flagellar clockwise rotation in bacterial envelopes by insertion of the chemotaxis protein CheY. *Proc. Natl. Acad. Sci. U.S.A.* **83**, 7157–7161 (1986).
6. D. A. Sanders, B. L. Gillece-Castro, A. M. Stock, A. L. Burlingame, D. E. Koshland, Identification of the site of phosphorylation of the chemotaxis response regulator protein, CheY*. *J. Biol. Chem.* **264**, 21770–21778 (1989).
7. N. R. Francis, G. E. Sosinsky, D. Thomas, D. J. DeRosier, Isolation, characterization and structure of bacterial flagellar motors containing the switch complex. *J. Mol. Biol.* **235**, 1261–1270 (1994).
8. M. K. Sarkar, K. Paul, D. Blair, Chemotaxis signaling protein CheY binds to the rotor protein FliN to control the direction of flagellar rotation in *Escherichia coli*. *Proc. Natl. Acad. Sci. U.S.A.* **107**, 9370–9375 (2010).
9. J. Yuan, R. W. Branch, B. G. Hosu, H. C. Berg, Adaptation at the output of the chemotaxis signalling pathway. *Nature* **484**, 233–U115 (2012).
10. P. P. Lele, R. W. Branch, V. S. J. Nathan, H. C. Berg, Mechanism for adaptive remodeling of the bacterial flagellar switch. *Proc. Natl. Acad. Sci. U.S.A.* **109**, 20018–20022 (2012).
11. A. Bren, M. Eisenbach, The N terminus of the flagellar switch protein, FliM, is the binding domain for the chemotactic response regulator, CheY. *J. Mol. Biol.* **278**, 507–514 (1998).
12. T. A. Duke, N. Le Novère, D. Bray, Conformational spread in a ring of proteins: A stochastic approach to allostery. *J. Mol. Biol.* **308**, 541–553 (2001).
13. H. Fukuoka, T. Sagawa, Y. Inoue, H. Takahashi, A. Ishijima, Direct imaging of intracellular signaling components that regulate bacterial chemotaxis. *Sci. Signal.* **7**, ra32 (2014).
14. Y. Chang *et al.*, Molecular mechanism for rotational switching of the bacterial flagellar motor. *Nat. Struct. Mol. Biol.* **27**, 1041–1047 (2020).
15. P. K. Singh *et al.*, CryoEM structures reveal how the bacterial flagellum rotates and switches direction. *Nat. Microbiol.* **9**, 1271–1281 (2024).
16. P. Cluzel, M. Surette, S. Leibler, An ultrasensitive bacterial motor revealed by monitoring signaling proteins in single cells. *Science* **287**, 1652–1655 (2000).
17. J. Yuan, H. C. Berg, Ultrasensitivity of an adaptive bacterial motor. *J. Mol. Biol.* **425**, 1760–1764 (2013).
18. F. Rieke, D. Baylor, Single-photon detection by rod cells of the retina. *Rev. Mod. Phys.* **70**, 1027–1036 (1998).
19. S. Hecht, S. Shlaer, M. H. Pirenne, Energy, quanta, and vision. *J. Gen. Physiol.* **25**, 819–840 (1942).
20. H. Barlow, Retinal noise and absolute threshold. *J. Opt. Soc. Am.* **46**, 634–639 (1956).
21. B. Sakitt, Counting every quantum. *J. Physiol.* **223**, 131–150 (1972).
22. D. A. Baylor, T. D. Lamb, K. W. Yau, Responses of retinal rods to single photons. *J. Physiol.* **288**, 613–634 (1979).
23. E. Korobkova, T. Emonet, J. M. G. Vilar, T. S. Shimizu, P. Cluzel, From molecular noise to behavioural variability in a single bacterium. *Nature* **428**, 574–578 (2004).
24. T. Emonet, P. Cluzel, Relationship between cellular response and behavioral variability in bacterial chemotaxis. *Proc. Natl. Acad. Sci. U.S.A.* **105**, 3304–3309 (2008).

25. O. Hoeller, D. Gong, O. D. Weiner, How to understand and outwit adaptation. *Dev.l Cell* **28**, 607–616 (2014).
26. S. M. Block, J. E. Segall, H. C. Berg, Impulse responses in bacterial chemotaxis. *Cell* **31**, 215–226 (1982).
27. J. Segall, S. Block, H. Berg, Temporal comparisons in bacterial chemotaxis. *Proc. Natl. Acad. Sci. U.S.A.* **83**, 8987–8991 (1986).
28. K. Lipkow, S. Andrews, D. Bray, Simulated diffusion of phosphorylated CheY through the cytoplasm of *Escherichia coli*. *J. Bacteriol.* **187**, 45–53 (2005).
29. S. Crosson, S. Rajagopal, K. Moffat, The LOV domain family: Photoresponsive signaling modules coupled to diverse output domains. *Biochemistry* **42**, 2–10 (2003).
30. B. D. Zoltowski, K. H. Gardner, Tripping the light fantastic: Blue-light photoreceptors as examples of environmentally modulated protein-protein interactions. *Biochemistry* **50**, 4–16 (2011).
31. T. E. Swartz *et al*., The photocycle of a flavin-binding domain of the blue light photoreceptor phototropin. *J. Biol. Chem.* **276**, 36493–36500 (2001).
32. J. M. Christie *et al*., Steric interactions stabilize the signaling state of the LOV2 domain of phototropin 1. *Biochemistry* **46**, 9310–9319 (2007).
33. F. Kawano, Y. Aono, H. Suzuki, M. Sato, Fluorescence imaging-based high-throughput screening of fast- and slow-cycling LOV proteins. *PLoS One* **8**, e82693–e82693 (2013).
34. S. Hemmer *et al*., Machine learning-assisted engineering of light, oxygen, voltage photoreceptor adduct lifetime. *JACS* **3**, 3311–3323 (2023).
35. A. Vrabioiu, T. Mitchison, Structural insights into yeast septin organization from polarized fluorescence microscopy. *Nature* **443**, 466–469 (2006).
36. L. He *et al*., Circularly permuted LOV2 as a modular photoswitch for optogenetic engineering. *Nat. Chem. Biol.* **17**, 915–923 (2021).
37. L. Geng, J. Shen, W. Wang, Circularly permuted AsLOV2 as an optogenetic module for engineering photoswitchable peptides. *Chem. Commun.* **57**, 8051–8054 (2021).
38. J. Jumper *et al*., Highly accurate protein structure prediction with AlphaFold. *Nature* **596**, 583–589 (2021).
39. S. L. Porter, G. H. Wadhams, J. P. Armitage, Signal processing in complex chemotaxis pathways. *Nat. Rev. Microbiol.* **9**, 153–165 (2011).
40. M. D. Baker, P. M. Wolanin, J. B. Stock, Signal transduction in bacterial chemotaxis. *BioEssays* **28**, 9–22 (2006).
41. U. Alon *et al*., Response regulator output in bacterial chemotaxis. *EMBO J.* **17**, 4238–4248 (1998).
42. J. H. Davis, A. J. Rubin, R. T. Sauer, Design, construction and characterization of a set of insulated bacterial promoters. *Nucleic Acids Res.* **39**, 1131–1141 (2011).
43. H. C. Berg, Dynamic properties of bacterial flagellar motors. *Nature* **249**, 77–79 (1974).
44. M. T. Brown *et al*., Flagellar hook flexibility is essential for bundle formation in swimming *Escherichia coli* cells. *J. Bacteriol.* **194**, 3495–3501 (2012).
45. D. Beckett, E. Kovaleva, P. J. Schatz, A minimal peptide substrate in biotin holoenzyme synthetase-catalyzed biotinylation. *Protein Sci.* **8**, 921–929 (1999).
46. X. Yao, M. K. Rosen, K. H. Gardner, Estimation of the available free energy in a LOV2-Jα photoswitch. *Nat. Chem. Biol.* **4**, 491–497 (2008).
47. D. Strickland *et al*., Rationally improving LOV domain-based photoswitches. *Nat. Methods* **7**, 623–626 (2010).
48. A. B. Benedict, J. D. Chamberlain, D. G. Calvopina, J. S. Griffitts, Translation initiation from sequence variants of the bacteriophage t7 g10rbs in *E. coli* and *Agrobacterium fabrum*. *Mol. Biol. Rep.* **49**, 833–838 (2022).
49. S. Johnson *et al*., Structural basis of directional switching by the bacterial flagellum. *Nat. Microbiol.* **9**, 1282–1292 (2024).
50. J. J. Hopfield, Kinetic proofreading: A new mechanism for reducing errors in biosynthetic processes requiring high specificity. *Proc. Natl. Acad. Sci. U.S.A.* **71**, 4135–4139 (1974).
51. W. Marwan, P. Hegemann, D. Oesterhelt, Single photon detection by an archaebacterium. *J. Mol. Biol.* **199**, 663–664 (1988).
52. M. J. Schnitzer, S. M. Block, Statistical kinetics of processive enzymes. *Cold Spring Harb. Symp. Quant. Biol.* **60**, 793–802 (1995).
53. Y. Zhou, X. Zhuang, Kinetic analysis of sequential multistep reactions. *J. Phys. Chem. B* **111**, 13600–13610 (2007).
54. D. L. Floyd, S. C. Harrison, A. M. van Oijen, Analysis of kinetic intermediates in single-particle dwell-time distributions. *Biophys. J.* **99**, 360–366 (2010).
55. Q. Ma, D. V. N. Jr., P. K. Maini, R. M. Berry, F. Bai, Conformational spread in the flagellar motor switch: A model study. *PLoS Comput. Biol.* **8**, e1002523 (2012).
56. V. Sourjik, H. C. Berg, Binding of the *Escherichia coli* response regulator CheY to its target measured in vivo by fluorescence resonance energy transfer. *Proc. Natl. Acad. Sci. U.S.A.* **99**, 12669–12674 (2002).
57. A. F. Bitbol, N. S. Wingreen, Fundamental constraints on the abundances of chemotaxis proteins. *Biophys. J.* **108**, 1293–1305 (2015).
58. P. P. Lele, B. G. Hosu, H. C. Berg, Dynamics of mechanosensing in the bacterial flagellar motor. *Proc. Natl. Acad. Sci. U.S.A.* **110**, 11839–11844 (2013).
59. J. D. Antani *et al*., Mechanosensitive recruitment of stator units promotes binding of the response regulator CheY-p to the flagellar motor. *Nat. Commun.* **12**, 5442 (2021).
60. Y. S. Dufour, X. Fu, L. Hernandez-Nunez, T. Emonet, Limits of feedback control in bacterial chemotaxis. *PLoS Comput. Biol.* **10**, e1003694 (2014).
61. N. W. Frankel *et al*., Adaptability of non-genetic diversity in bacterial chemotaxis. *eLife* **3**, e03526 (2014).
62. A. J. Waite *et al*., Non-genetic diversity modulates population performance. *Mol. Syst. Biol.* **12**, 895 (2016).
63. J. Long, S. W. Zucker, T. Emonet, Feedback between motion and sensation provides nonlinear boost in run-and-tumble navigation. *PLoS Comput. Biol.* **13**, e1005429 (2017).
64. C. S. Barker, B. M. Pruss, P. Matsumura, Increased motility of *Escherichia coli* by insertion sequence element integration into the regulatory region of the flhD operon. *J. Bacteriol.* **186**, 7529–7537 (2004).
65. K. A. Datsenko, B. L. Wanner, One-step inactivation of chromosomal genes in *Escherichia coli* k-12 using PCR products. *Proc. Natl. Acad. Sci. U.S.A.* **97**, 6640–6645 (2000).
66. E. Balleza, J. M. Kim, P. Cluzel, Systematic characterization of maturation time of fluorescent proteins in living cells. *Nat. Methods* **15**, 47–51 (2018).
67. E. Amann, B. Ochs, K. J. Abel, Tightly regulated tac promoter vectors useful for the expression of unfused and fused proteins in *Escherichia coli*. *Gene* **69**, 301–315 (1988).
68. A. M. Vrabioiu, The dynamic response of the bacterial flagellar motor to its direct intracellular input signal. Zenodo. https://zenodo.org/records/18635165.
69. A. M. Vrabioiu, Plasmids. Addgene. https://www.addgene.org/depositing/87241/. Deposited 16 February 2026.